Heat transport in silicon from first-principles calculations

Keivan Esfarjani and Gang Chen
Department of Mechanical Engineering, Massachusetts Institute of Technology, 77 Massachusetts Avenue, Cambridge, Massachusetts 02139, USA

Harold T. Stokes
Department of Physics, Brigham Young University, Salt Lake City, Utah 84602, USA
(Received 30 March 2011; revised manuscript received 13 June 2011; published 23 August 2011)

Using harmonic and anharmonic force constants extracted from density functional calculations within a supercell, we have developed a relatively simple but general method to compute thermodynamic and thermal properties of any crystal. First, from the harmonic, cubic, and quartic force constants, we construct a force field for molecular dynamics. It is exact in the limit of small atomic displacements and thus does not suffer from inaccuracies inherent in semiempirical potentials such as Stillinger-Weber's. By using the Green-Kubo formula and molecular dynamics simulations, we extract the bulk thermal conductivity. This method is accurate at high temperatures where three-phonon processes need to be included to higher orders, but may suffer from size scaling issues. Next, we use perturbation theory (Fermi golden rule) to extract the phonon lifetimes and compute the thermal conductivity κ from the relaxation-time approximation. This method is valid at most temperatures, but will overestimate κ at very high temperatures, where higher-order processes neglected in our calculations also contribute. As a test, these methods are applied to bulk crystalline silicon, and the results are compared and differences are discussed in more detail. The presented methodology paves the way for a systematic approach to model heat transport in solids using multiscale modeling, in which the relaxation time due to anharmonic three-phonon processes is calculated quantitatively, in addition to the usual harmonic properties such as phonon frequencies and group velocities. It also allows the construction of an accurate bulk interatomic potentials database.

DOI: 10.1103/PhysRevB.84.085204 PACS number(s): 63.20.Ry, 63.20.kg, 44.10.+i

I. INTRODUCTION

Classical molecular dynamics (MD) simulations use either semiempirical potentials such as Stillinger-Weber (SW),[1] Abell-Tersoff-Brenner,[2] or other type of force fields where the potential energy is an analytical function of the atomic positions, or first-principles potentials calculated typically using density functional methods based on either the Born-Oppenheimer[3] or the Car-Parrinello[4] dynamics. The former are fast to compute but suffer from inaccuracies, while the latter are accurate but time consuming to compute. Due to recent interest in thermal transport in semiconductor materials having good thermoelectric properties and in the topic of microelectronics thermal management in general, there have been many calculations of the lattice thermal conductivity of materials using the Green-Kubo (GK) formula.[5,6] This formula relates the thermal conductivity, through the use of the fluctuation-dissipation theorem, to the time integral of the heat-current autocorrelation function. The latter is calculated from an MD simulation, and the ensemble average is usually replaced by a time average. Semiempirical potentials such as SW are usually used to perform the MD simulation for a system such as Si. As the thermal conductivity of a perfect crystal is mainly due to anharmonic three-phonon processes, directly related to the third derivatives of the potential energy with respect to atomic displacements, and the latter is generally not fitted or considered in the design of the semiempirical potentials, there is really no good reason to expect an accurate value for the thermal conductivity calculated from a GK-MD simulation. In the case of Si, when using the SW potential, however, for some reason,[7] relatively good agreement is found between the experiment and the simulation results, even for a relatively small supercell.[8–11] The latter fact is also cause for concern because, as we will show in the following, a small supercell limits the number of long-wavelength phonons that carry a large portion of the heat in a material. The lucky agreement can be attributed to a cancellation due to two different effects, which will be discussed in Sec. III B. Sellan *et al.*[11] have presented a discussion on convergence issues, mostly with respect to nonequilibrium MD simulations, and we will also discuss the scaling issue with respect to GK-MD and lattice dynamics (LD) in this paper.

More accurate calculations of the thermal conductivity, based on the full solution of the Boltzmann transport equation, have shown that the thermal conductivity of Si using the SW potential is about four times larger than the experiment, while using the Tersoff or environment-dependent interaction potentials (EIDPs) produces results that are about twice as large as the experimental values.[12] In a similar work, using the EDIP, Pascual-Gutierrez *et al.*[13] also found thermal conductivity of bulk Si from MD in good agreement with experiments. In a subsequent work,[14] the same group computed the thermal conductivity using the lattice dynamics (LD) theory based on the same EDIP, similar to the work of Broido *et al.*[12] They obtained good agreement with experiments, whereas Broido *et al.* did not. The reason for this discrepancy, as they also mention in their paper, is unclear. Opinions on the accuracy of semiempirical potentials seem to differ, as there have been other reports[15] where SW is found to overestimate the thermal conductivity by 70%. As we will show in this paper,

some of these potentials might not be completely reliable for the calculation of the thermal transport properties for the simple reason that they were not fitted or constructed to have the correct third derivatives, which are responsible for the thermal resistivity of a material. In fact, even their harmonic-force constants produce phonon dispersions and elastic constants which differ from experiments by 10% up to 40%. Furthermore, such potentials exist and have been thoroughly tested for only a very small number of pure crystalline solids.

In a tour de force calculation work, Broido *et al*. later used the density functional perturbation theory (DFPT) formalism in order to calculate the phonon-scattering rates from first-principles DFT calculations, and were able to successfully reproduce the thermal conductivity of bulk Si and Ge.[16] Their approach, which was very accurate, included the calculation of all the cubic force constants up to seventh nearest neighbor, and the complete iterative solution of the Boltzmann transport equation.

We recently developed a methodology to extract second, third, and fourth derivatives of the potential energy from first-principles calculations,[17] and showed that the phonon-dispersion relation in Si can be well reproduced. In this paper, we pursue this work further and use these derivatives to construct a force field in order to explore the results from MD simulations and perturbation calculations to calculate the thermal conductivity of bulk Si. We should mention that our approach, even though very similar in essence to that of Broido *et al*., is simpler in the sense that it limits the range of the force constants (FCs) to a few neighbors (5 for harmonic and 1 for cubic in the present case study of Si, in contrast to more than 20 for harmonic and 7 for cubic in the work of Broido *et al*.).[16] For the sake of physical correctness, however, we enforce the translational, rotational, and Huang invariances[18] on the extracted force constants. So the latter are not exactly equal to the ones obtained from DFPT or any finite difference calculation of the forces, but make the calculation load much lighter than if one had to include so many neighbors. On the other hand, a DFPT calculation, if restricted to few neighbors, should enforce all these invariances. Usually only the translational ones, also known as the acoustic sum rule (ASR), are enforced in some of the standard DFT codes such as QUANTUM ESPRESSO.[19]

In what follows, we briefly review the methodology to extract force constants from first-principles density functional theory calculations (FP-DFT). The formalism for the molecular dynamics and Green-Kubo calculations of κ are explained in Sec. III. This will be followed by the lattice-dynamics approach detailed in Sec. IV. Results for Si will be shown and discussed in Sec. V, followed by conclusions.

II. EXTRACTION OF FORCE CONSTANTS FROM FP-DFT CALCULATIONS

We construct the potential energy V for the MD simulation as a Taylor expansion up to the fourth order in the atomic displacement u_i of atom i about its equilibrium position,

$$V = V_0 + \sum_i \Pi_i u_i + \frac{1}{2!}\sum_{ij} \Phi_{ij}\, u_i u_j + \frac{1}{3!}\sum_{ijk} \Psi_{ijk}\, u_i u_j u_k + \frac{1}{4!}\sum_{ijkl} \chi_{ijkl}\, u_i u_j u_k u_l \quad (1)$$

$$= \sum_i \left(e_i - \frac{1}{2} m_i v_i^2 \right). \quad (2)$$

The last equation defines the on-site energy e_i. If the displacements u_i are around the equilibrium position, and this is usually the case, then $\Pi_i = 0$. The coefficients Φ, Ψ, and χ in the expansion are called the harmonic, cubic, and quartic force constants, respectively, and satisfy certain symmetry constraints. Namely, they must be invariant under the interchange of the indices, uniform translations, and rotations of the atoms, in addition to under symmetry operations of the crystal. The details of the needed constraints and how they are imposed can be found in our previous work.[17]

To get these numbers, we consider one or several supercells in which atoms are in their equilibrium position. One, two, or three neighboring atoms are moved simultaneously by a small amount, typically about 0.01 Å along the Cartesian directions. Consideration of crystal symmetry usually reduces the needed displacements. For instance, in a cubic-based crystal such as silicon, where the two atoms in the primitive cell are equivalent, one only needs to move one Si atom along the x direction. This is sufficient to extract all harmonic force constants if the supercell size is large enough. The latter size is chosen depending on the available computational power and the considered range of force constants. To get three- and four-body interaction terms, one needs to move two and three atoms at a time and record the forces on all atoms in the supercell. It is advantageous to record forces for atomic displacements in two opposite directions, as there would be cancellation of the cubic contributions and this would make the calculation of the harmonic FCs much more accurate (up to order u^2). Thus one would obtain a large set of force-displacement relations computed from a FP-DFT code. Together with the invariance constraints, an overcomplete linear set of equations on all the force constants will be formed. A singular-value decomposition algorithm is then used to solve this linear overcomplete set. We find that usually the violation of the invariance relations is of the order of 10^{-6} times the FC itself. This, however, requires a very accurate evaluation of the forces, meaning that they should have converged with respect to the cutoff energy and number of k-points to within at least four significant figures, if not more. Our experience on graphene[20] and silicon (present work and Ref. 17) has shown that the harmonic force constants are usually reproduced quite accurately. Higher-order FCs have less accuracy, as their contribution shows up in the second, third, or fourth significant figures of the forces. The main approximation is in cutting off the range of the interactions, which will lead to inaccuracies in some of the Gruneisen parameters, as we will shortly see.

III. MOLECULAR DYNAMICS AND THE GREEN-KUBO FORMALISM

Typically a supercell is constructed with periodic boundary conditions, and an MD simulation is performed over long enough time steps in order to reach thermal equilibrium, followed by a long (*N*,*V*,*E*) simulation in order to collect data on J for later statistical processing, i.e, time and ensemble averaging of its autocorrelation.

Based on the potential displayed in Eq. (2), one can extract the expression for the force required in the MD simulations,

$$F_i = -\sum_j u_j \left(\Phi_{ij} + \frac{1}{2!}\sum_k \Psi_{ijk}\, u_k + \frac{1}{3!}\sum_{kl} \chi_{ijkl}\, u_k u_l \right).$$

The heat current is defined in the discrete (atomic) case of a lattice, where there is no convection, as

$$J^\alpha = \sum_i J_i^\alpha = \sum_i \frac{d\left(e_i r_i^\alpha\right)}{dt} = \sum_{ij} \left(R_i^\alpha - R_j^\alpha\right)\left(v_j \cdot \frac{\partial e_i}{\partial u_j}\right), \tag{3}$$

where v_i is the velocity of particle i, and e_i, as defined in Eq. (2), is the local energy of atom i. Using our expansion, it can be expressed as a function of the force constants as follows (as we expand around the equilibrium position, we assume $\Pi_i = 0$):

$$e_i = \frac{1}{2} m_i v_i^2 + \frac{u_i}{2}\sum_j \left[\Phi_{ij}\, u_j + \frac{1}{3}\sum_k \Psi_{ijk}\, u_j u_k + \frac{1}{12}\sum_{ijkl} \chi_{ijkl}\, u_j u_k u_l \right]. \tag{4}$$

This definition leads to the following form of the local heat current:

$$J_i^\alpha = \frac{1}{2}\sum_j \left(R_i^\alpha - R_j^\alpha\right)\left[v_j \cdot u_i \left(\Phi_{ij} + \frac{2}{3}\sum_k \Psi_{ijk}\, u_k + \frac{1}{4}\sum_{kl} \chi_{ijkl}\, u_k u_l \right)\right]. \tag{5}$$

Finally, the thermal conductivity tensor is given by the well-known Green-Kubo relation,[5,6]

$$\kappa_{\alpha\beta} = \frac{1}{V k_B T^2}\int_0^\infty \langle J^\alpha(0) J^\beta(t)\rangle dt, \tag{6}$$

where $\alpha,\beta = x,y,z$, and $\langle A\rangle$ denotes the equilibrium average of the observable A, which in the classical case can be replaced by its time average provided the time is *long enough to satisfy ergodicity*. The ensemble averaging is necessary as long as different runs starting with different initial conditions lead to different integrated autocorrelation functions. The true current autocorrelations decay quite fast. In a single MD run, however, this decay is not observed. Instead, one observes a decay in the amplitude followed by random oscillations about zero. As finite systems are usually not ergodic, an ensemble average over the random initial conditions is also needed to correctly simulate the equilibrium average required in the Green-Kubo formula. In this case, the ensemble-averaged autocorrelation function will decay smoothly to zero with time. One will then see that the decay is indeed relatively short because the long-time tails get canceled after ensemble averaging. The advantage of the ensemble averaging, in addition of course to the usual time averaging, is that one samples the phase space more randomly and generates *uncorrelated* sets of pairs, $J^\alpha(0)J^\beta(t)$, for a given time difference t. In this case, the mean has the convergence properties of Gaussian-distributed variables, and the error decays to zero as the inverse square root of the number of initial conditions.

In a numerical simulation, the GK formula should be replaced by

$$\kappa_{\alpha\beta} = \frac{1}{V_{\text{cell}}\, k_B T^2}\frac{1}{N_{\text{ens}}}\sum_{i=1}^{N_{\text{ens}}}\frac{\Delta t}{\mathcal{T}}\left[\sum_{t=0}^{\mathcal{T}}\sum_{p=1}^{\mathcal{T}-t+1} J_i^\alpha(p) J_i^\beta(p+t)\right], \tag{7}$$

where $\mathcal{T}$ is the total simulation time of each run, Δt is the time difference between two successive data points, t and p are integers labeling time, and N_{ens} is the number of generated initial conditions, each labeled by i. One important comment is in order here, and that is the use of $1/\mathcal{T}$ in the denominator instead of the more intuitive $1/(\mathcal{T}-t+1)$, which is the actual number of terms in the last sum. One can show that the choice in Eq. (7) provides an unbiased estimator of the autocorrelation.[21] Some previous works in the GK method, such as Ref. 9, have used the "biased" formula, which would be fine as long as the total simulation time is much larger than the largest time t used for the integration. One simple way to become convinced that Eq. (7) is the correct way is to consider large times t near the maximum simulation time $\mathcal{T}$. As $J(p)$ and $J(p+t)$ are both fluctuating random numbers, and there are not enough terms in the sum to make the average go to zero, the time average will become large again and tend to $\sigma_J = \langle J(0)J(0)\rangle$ instead of decaying to zero as t approaches $\mathcal{T}$. A division by the small number $\mathcal{T}-t$ would not solve the problem, whereas the division by $\mathcal{T}$ would make this very small, as it should.

Because the simulation time $\mathcal{T}$ is usually quite long, the statistical error in the time averaging is usually small, and we estimate the error bars in our data from the ensemble averaging: If $\bar{C}(t)$ is the ensemble-averaged autocorrelation function, its error bar ΔC is evaluated as $\Delta C(t) = \{\sum_{i=1}^{N_{\text{ens}}}[C_i(t) - \bar{C}(t)]^2\}^{1/2}/N_{\text{ens}}$.

The magnitude of this error bar and the required accuracy in the results determine how many ensembles are needed for a proper estimation of thermal conductivity.

A. Number of necessary MD steps

For a given supercell size, there is a discrete number of phonon modes which can propagate and get scattered in the system. The largest wavelength consistent with the periodic boundary conditions would be the supercell length. To this, one can correspond a smallest phonon wave number or frequency allowed in the simulation: $\omega_{\text{cut}} = 2\pi c/L$. The total simulation time should be large enough so that all phonon modes can get scattered a few times within the simulation period. The largest relaxation times belong to acoustic modes and usually decay as the inverse square of the phonon frequency. By knowing the smallest allowed frequency ω_{cut} due to the finite size of the

system, one can estimate the corresponding phonon lifetime [using Klemens' formula displayed in Eq. (8), for instance]. The total MD simulation time should, therefore, be a few times larger than the largest phonon lifetime so that scattering events of long-wavelength phonon modes can properly be sampled during the MD run. As an example, we can consider a Si system in a cubic $10 \times 10 \times 10$ supercell of 8000 atoms. In this case, $L = 10 \times 5.4$ Å $= 5.4$ nm, corresponding to $k_c = 2\pi/10a$, which is a fifth of the $\Gamma \rightarrow X$ line. The lowest frequency mode is therefore about $\omega_{\rm cut} = 1$ THz. As can be seen in Fig. 5, the normal and umklapp lifetimes at this frequency are 3000 and 10 000 ps, respectively, leading to a total lifetime of 2300 ps. So in order to sample such rare events, one needs to calculate the autocorrelation over at least 20 ns, which means the MD simulation should be run for at least the same amount of time, if not longer. This could be computationally prohibitive. If the runs are made with fewer MD steps, long-wavelength phonons will not be relaxed and the autocorrelation will not tend to zero. Another consequence of this case is that for large supercells, as relaxation times scale as $1/\omega_{\rm cut}^2 \propto L^2$, longer simulation times proportional to the *square* of the the supercell size will be required.

B. Size scaling

As mentioned, the choice of a finite supercell comes with the cost of discretizing the phonon modes and suppressing the phonons of wavelengths longer than the supercell length. The neglected contribution may be estimated as follows: the anharmonic lifetime of acoustic modes may be approximated by the Klemens' formula[22]

$$\frac{1}{\tau_{k\lambda}^{\rm Klemens}} = \gamma_{k\lambda}^2 \frac{2k_B T}{M\, v_{k\lambda}^2} \frac{\omega_{k\lambda}^2}{\omega_\lambda^{\rm max}}, \tag{8}$$

where $\omega_\lambda^{\rm max}$ is the largest frequency of the branch λ, $\gamma_{k\lambda}$ is the mode Gruneisen parameter, $\omega_{k\lambda}$ is the frequency, and $v_{k\lambda}$ is the group velocity associated with the mode $k\lambda$. Therefore, long-wavelength phonons will have a large relaxation time and can considerably contribute to the thermal conductivity. By assuming this form in the relaxation-time approximation to the thermal conductivity and using Eq. (16), we can write the thermal conductivity as a sum over the contributions of phonons of different frequencies as

$$\kappa = \int_0^\infty \frac{1}{3}\tau(\omega)v^2(\omega)C_v(\omega){\rm DOS}(\omega)\, d\omega.$$

In three dimensions (3D), since the density of states (DOS) is quadratic in frequency, the contribution of long-wavelength acoustic phonons would be linear in the cutoff frequency $\omega_{\rm cut} = 2\pi c/L$,

$$\kappa(L) = \kappa(\infty) - \int_0^{\omega_{\rm cut}} \frac{1}{3}\tau(\omega)v^2(\omega)C_v(\omega){\rm DOS}(\omega)\, d\omega.$$

For low frequencies, $C_v(\omega) = k_B[\beta\hbar\omega/2\sinh(\beta\hbar\omega/2)]^2 \simeq k_B$ and $v(\omega) \simeq c$, so that

$$\kappa(L) = \kappa(\infty) - A\int_0^{\omega_{\rm cut}} \frac{1}{\omega^2}{\rm DOS}(\omega)\, d\omega = \kappa(\infty) - D\omega_{\rm cut}$$
$$= \kappa(\infty) - E\frac{1}{L} = \kappa(\infty) - F/\sqrt{\Lambda_c}, \tag{9}$$

where A, D, E, and F are constants that do not depend on the size, and Λ_c is the mean-free path (MFP) associated with the cutoff frequency $\omega_{\rm cut} = 2\pi c/L$. This gives us a way to deduce how the thermal conductivity of a finite-size sample scales with the supercell length L or the cutoff frequency $\omega_{\rm cut}$ or the MFP Λ_c. We should note that a different scaling law $[1/\kappa(L) = 1/\kappa(\infty) + C/L]$ was proposed and used by Sellan *et al.*[11] and also Turney *et al.*[23] to extrapolate their thermal conductivity data to infinite size. The argument they used to deduce it, however, was based on Matthiesen's rule, stating that the bulk resistivity is obtained by adding the finite-size resistivity to the one obtained from L/v taken as the relaxation time.

There is an additional problem with finite-size MD simulations. Even though momentum is still conserved in a three-phonon process, because the modes are *discrete* in a finite supercell, energy conservation will not always be possible, unless the energy difference $\omega - \omega_1 - \omega_2 \leqslant \Gamma$, where Γ is on the order of the sum of inverse lifetimes of the three considered phonons. If this relation is not satisfied, the considered three-phonon scattering will not take place in a finite supercell, and this will lead to an overestimation of the lifetime of the phonons and, thus, of the thermal conductivity.

These competing effects, namely, an overestimation of κ due to limited phase space for energy conservation and an underestimation due to the cutoff of low-frequency acoustic modes, may lead to a magical cancellation, resulting in thermal conductivities in good agreement with experiments even for moderate supercell size. This error cancellation will likely affect the temperature dependence of κ: at higher temperatures, the discreteness error is reduced as Γ increases linearly with T. The frequency cutoff error, however, will not be affected by high temperatures. Consequently, as T is increased, the thermal conductivity of a finite sample will decrease faster than $1/T$ with temperature. This has been observed in the work of Volz and Chen.[8] It can also be verified by introducing other scattering events, such as isotope or defect scattering, leading to larger Γ values. In such cases, the discreteness of modes will have little effect, and the simulated κ will be less than the exact one due to the effect of the cutoff of long MFP phonons. As a result, in a system where scattering rates are high due to disorder or high temperatures, GK-MD simulations will typically require larger supercells to converge.

The correct way of estimating $\kappa(T)$ is to do a proper size scaling at each temperature by plotting $\kappa(T, L)$ versus $1/L$, and linearly extrapolating to $1/L \rightarrow 0$.

IV. THE LATTICE DYNAMICS APPROACH

Using the extracted force constants, one can form the dynamical matrix of the crystal using its primitive cell data,

$$D_{\tau\tau'}^{\alpha\beta}(k) = \sum_R \frac{1}{\sqrt{M_\tau M_{\tau'}}} \Phi_{0\tau,R\tau'}^{\alpha\beta} e^{ik\cdot R}, \tag{10}$$

where R is a translation vector of the crystal, τ refers to an atom in the primitive cell, and α, β are Cartesian components x, y, z. Such sums of the force constants over the translation vectors of the primitive lattice are usually short ranged and fast to compute, except when Coulomb interactions are involved, in which case the sum is evaluated using the Ewald method.

By diagonalizing this matrix, one can find the phonon spectrum and the normal modes as its eigenvectors,

$$\sum_{\tau'\beta} D^{\alpha\beta}_{\tau\tau'}(k)\, e^{\tau'\beta}_{\lambda}(k) = \omega^2_{k\lambda}\, e^{\tau\alpha}_{\lambda}(k), \tag{11}$$

where λ labels a phonon band (or branch), and k refers to a point in the first Brillouin zone (FBZ). Using these eigenvectors and eigenvalues, and from perturbation theory, one can calculate the phonon line shifts and lifetimes as the real and imaginary parts of the three-phonon self-energy defined as[24–27]

$$\Sigma(q\lambda,\omega) = -\frac{1}{2\hbar^2 N_k} \sum_{1,2,\epsilon=\pm1} |V(q\lambda,1,2)|^2 \times \left[\frac{(1+n_1+n_2)}{\omega_1+\omega_2+\epsilon\omega_c} + \frac{(n_2-n_1)}{\omega_1-\omega_2+\epsilon\omega_c}\right], \tag{12}$$

where $\omega_c = \omega - i\eta$, ($\eta \simeq 0^+$) is a small infinitesimal number, which in practice is taken to be finite for a given k-point mesh size, n is the equilibrium Bose-Einstein distribution function, and 1 and 2 refer to modes $(q_1\lambda_1)$ and $(q_2\lambda_2)$, respectively. The three-phonon matrix element V, expressed as a function of the cubic force constants Ψ, is given by

$$V(q\lambda,1,2) = \left(\frac{\hbar}{2}\right)^{3/2} \sum_{R_i\tau_i\alpha_i} \Psi^{\alpha\beta\gamma}_{0\tau,R_1\tau_1,R_2\tau_2} \times \frac{e^{i(q_1\cdot R_1+q_2\cdot R_2)} e^{\tau\alpha}_{\lambda}(q) e^{\tau_1\alpha_1}_{\lambda_1}(q_1) e^{\tau_2\alpha_2}_{\lambda_2}(q_2)}{\left[M_\tau M_{\tau_1} M_{\tau_2} \omega_{q\lambda}\omega_1\omega_2\right]^{1/2}}. \tag{13}$$

The calculation of the self-energy would require a double sum over the q-points (labeled above by 1 and 2) in the FBZ. Due to the conservation of momentum, however, only terms with $q+q_1+q_2 = G$, with G being a reciprocal lattice vector, should be included in the above sum. In practice, therefore, this involves only a single summation. To get the phonon dispersion and lifetimes due to three-phonon scattering terms, one needs to solve $E = \omega_{k\lambda} + \Sigma'(k\lambda,E)$, where Σ' is the real part of the self-energy ($\Sigma = \Sigma' + i\Sigma''$). This equation needs to be solved iteratively. Since the shift is usually small, to leading order, one can use $E = \omega_{k\lambda} + \Sigma'(k\lambda,\omega_{k\lambda})$, i.e., one uses the on-shell frequency as the second argument of the self-energy. The same approximation will be used for the imaginary part giving the inverse lifetimes. The corresponding phonon lifetime will be given by $\tau_{k\lambda} = 1/2\Sigma''(k\lambda,\omega_{k\lambda})$. In the evaluation of the imaginary part Σ'', one encounters Dirac δ functions reflecting the conservation of energy in the three-phonon process, $\omega_{k\lambda} = \omega_1 \pm \omega_2$. In effect, from Eq. (12), it can be noticed that the δ function is substituted by a Lorentzian function of width η. The latter depends on the choice of the k-point mesh in the FBZ. A small value for η can be used for a fine mesh, while a coarse mesh requires larger values of η. Typically, η is chosen to be of the order of energy spacing in the joint density of states (JDOS) so that the latter is a smooth function of the frequency and does not display any oscillations with sharp peaks, which would appear if the width is too small,

$$\text{JDOS}(\omega) = \frac{1}{N_k}\sum_{1,2} \delta(\omega-\omega_1-\omega_2) + \delta(\omega-\omega_1+\omega_2). \tag{14}$$

The anharmonicity can be characterized by the Gruneisen parameters (GP). The force constant GP is defined as $\gamma_\phi = -d\ \ln\ \phi/2\ d\ \ln\ V$, where V is the volume. The mode GP is defined as $\gamma_{k\lambda} = -d\ \ln\ \omega_{k\lambda}/\ d\ \ln\ V$, where $\omega_{k\lambda}$ is the phonon frequency evaluated at the point $\vec{k}$ and band index λ. It gives the relative decrease in the phonon frequency as the volume is increased by 1%. From the Taylor expansion of the harmonic force constants in terms of the volume or the lattice parameter, one can calculate such change:

$$\gamma_{k\lambda} = -\frac{1}{6\omega^2_{k\lambda}} \sum_{1,2} \Psi^{\alpha\alpha_1\alpha_2}_{0\tau,R_1\tau_1,R_2\tau_2} \frac{e^{ik\cdot(R_2-R_1)}}{\left[M_{\tau_1}M_{\tau_2}\right]^{1/2}} \times X^{\alpha}_{0\tau}\, e^{\tau_1\alpha_1}_{\lambda}(-k)\, e^{\tau_2\alpha_2}_{\lambda}(k), \tag{15}$$

where $X_{R\tau}$ is the equilibrium atomic position of atom type τ in the primitive cell labeled by the translation vector R.

Finally, the thermal conductivity is calculated within the relaxation-time approximation (RTA), which leads to the following well-known expression for the thermal conductivity of an isotropic system:

$$\kappa = \frac{1}{3\mathbf{\Omega}N_k} \sum_{k\lambda} v^2_{k\lambda}\tau_{k\lambda}\hbar\omega_{k\lambda}\,\partial n_{k\lambda}/\partial T, \tag{16}$$

where $\mathbf{\Omega}$ is the volume of the unit cell. The relaxation time $\tau_{k\lambda}$ in this expression represents the time after which a phonon in mode $k\lambda$ reaches equilibrium on the average, and depends on the scattering processes involved. In a pure bulk sample, the only source of phonon scattering is anharmonicity dominated usually by three-phonon processes. Using perturbation theory or the well-known Fermi golden rule (FGR), one can derive the expression of the relaxation time as a function of the cubic force constants.[24–27] It can be shown that to a good approximation, it is given by

$$\tau_{q\lambda} \approx \frac{1}{2\Im[\Sigma(q\lambda,\omega_{q\lambda})]}. \tag{17}$$

In what follows, we have disregarded the boundary scattering term, which is responsible for the low-temperature behavior of κ. In such case, κ is expected to saturate to a finite value at low enough temperatures. The reason for this saturation can be understood if one assumes the low-frequency limit of the DOS and the relaxation times similar to Eq. (9). Considering that in $\omega \to 0$ limit, we have $\text{DOS}_\lambda(\omega) \to \omega^2/2\pi^2 c^3_\lambda$ and $C_v(\omega) = k_B(x/\text{sh}x)^2$ (with $x = \beta\hbar\omega/2$), and since normal processes dominate at low temperatures, the relaxation time can be written as $\tau(\omega) \to \hbar\omega_o^2/\omega^2 k_B T$, the integral defining the thermal conductivity can be transformed in the low-temperature limit to

$$\kappa(T) = \sum_{\lambda=\text{acoustic}} \frac{k_B\omega_o^2}{3\pi^2 c_\lambda}\int_0^\infty \left(\frac{x}{\text{sh}x}\right)^2 dx = \sum_{\lambda=\text{acoustic}} \frac{k_B\omega_o^2}{18c_\lambda}.$$

The constant ω_o that appears in the low-energy limit of the relaxation time as well as the speeds of sound c_λ determine the saturated value of the thermal conductivity. So when only three-phonon scattering processes are included, the thermal conductivity would tend to $\sum_{\lambda=\text{acoustic}} k_B\omega_o^2/18c_\lambda$ as T goes to 0.

Finally, in our numerical calculations where the integral in the FBZ has been approximated by a sum over a discrete set of k-points, the low-frequency region is not properly sampled and we observe a decrease at low T, and therefore have not reported the unreliable low-temperature data in this work.

V. RESULTS AND DISCUSSIONS

A. Validation of force constants

First-principles calculations were done using the PWSCF code of the QUANTUM ESPRESSO package.[19] A set of force-displacement data was calculated using a $2 \times 2 \times 2$ supercell of 64 Si atoms. The set of force-displacement data, along with the symmetry constraints, form an overcomplete linear set of equations needed to determine the potential derivatives. We use the local density approximation (LDA) of Perdew and Zunger[28] with a cutoff energy of 40 Ryd and 10 k-points in the irreducible Brillouin zone of the cubic supercell. The range of different ranks of force constants can be chosen by the user. We have set the range of harmonic force constants (FCs) to 5 nearest neighbor shells, and that of the cubic and quartic force constants to the first neighbor shell only. This results in 17, 5, and 14 independent harmonic, cubic, and quartic FCs, respectively. The corresponding number of terms in the Taylor expansion of the potential energy are, however, equal to 1500, 1146, and 7980, respectively. This is why the ranges were restricted to 5, 1, and 1 nearest-neighbor shells in order to limit the computational time to a reasonable amount. Note that despite the large number of terms to be computed, arithmetic operations are only limited to additions and multiplications.

In Fig. 1, we show the change in the total energy as an atom in the supercell is moved along the [100], [110], and [111] directions, respectively. Results from DFT calculations are compared against our developed force field including the harmonic, harmonic + cubic, and harmonic + cubic + quartic terms of the Taylor expansion. For the sake of comparison, we have also plotted the same energy change obtained from the Stillinger-Weber (SW) potential,[1] which is widely used in MD simulations of Si systems.

To further assess the accuracy of the force field, we have also moved all the atoms in the supercell in different random directions by a small amount of magnitudes 0.1 and 0.2 Å, respectively, and compared the average force of our model and the SW potential to the FP-DFT one. The deviation is characterized by

$$\sigma(\text{model}) = \frac{\sum_{i\alpha} \left(F_{i\alpha}^{\text{model}} - F_{i\alpha}^{\text{DFT}}\right)^2}{\sum_{i\alpha} F_{i\alpha}^{\text{DFT}\,2}}. \qquad (18)$$

The results for the parameter σ are summarized in Table I.

We note that this type of error estimate would also include contributions from many-body forces, and is a more stringent test on the force field. The errors from the present model are consistently about four to five times smaller that the SW potential.

TABLE I. Typical deviations in the SW and Taylor expansion (present model) force fields compared to true FP-DFT forces. They are obtained by moving all 64 atoms in the supercell in a random direction by 0.1 and 0.2 Å, respectively.

Amplitude (Å)	σ (SW)	σ (Present)
0.1	0.35	0.05
0.2	0.28	0.08

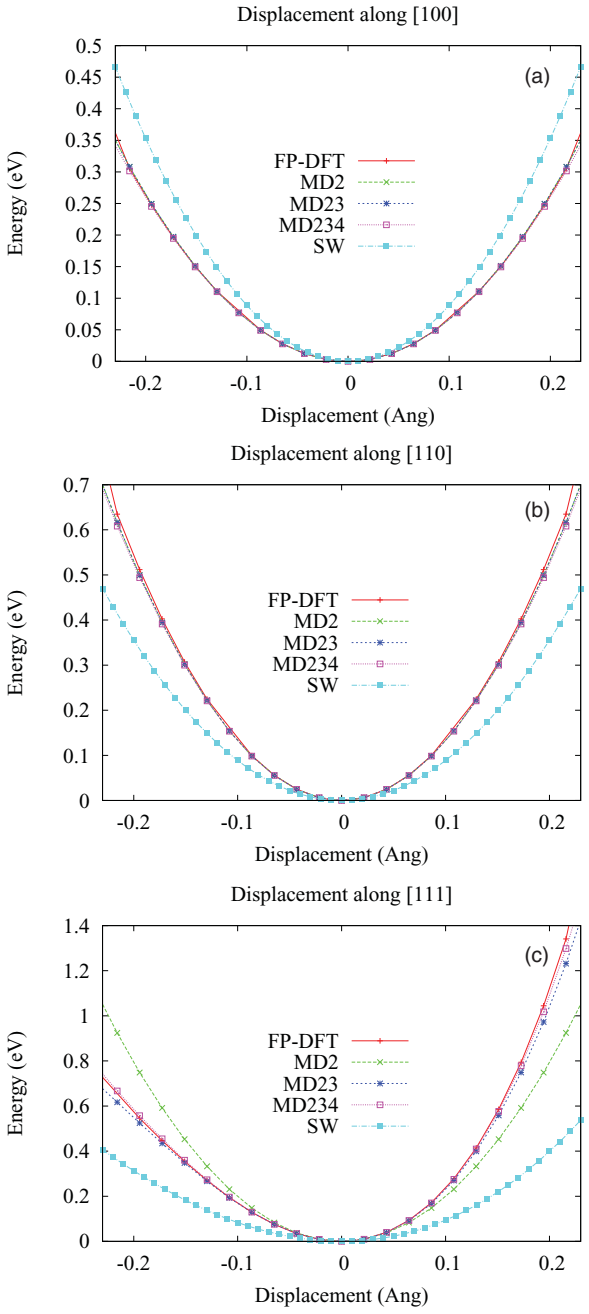

FIG. 1. (Color online) Total energy as an atom is moved in the (a) [100], (b) [110], and (c) [111] directions. DFT results are compared with the force field and the Stillinger-Weber potential. MD234 refers to the force field in which all harmonic, cubic, and quartic terms are included, while MD2 refers only to the harmonic force field, etc.

In the following, we follow two paths to compute the thermal conductivity. The first is to use the Green-Kubo formula by using the results from an MD simulation.

B. Thermal conductivity from GK-MD

As previously mentioned, there will be large fluctuations in the current autocorrelation function versus time from one run to the next, and therefore an averaging over several initial conditions is necessary to produce a reliable plot. In Fig. 2,

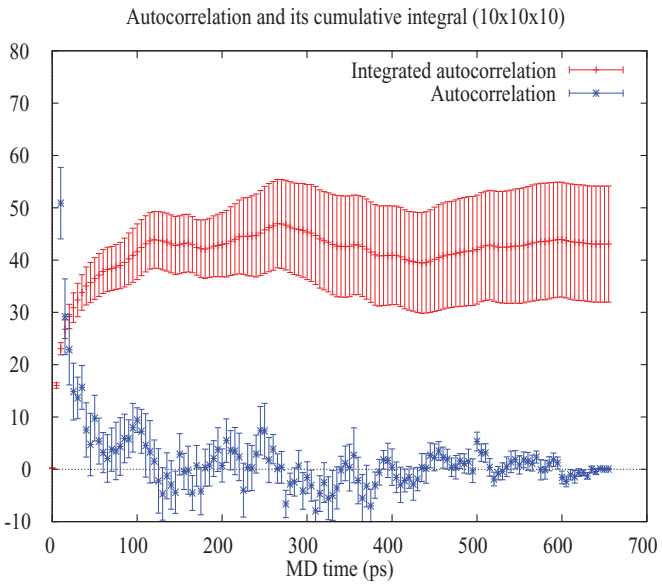

FIG. 2. (Color online) Plot of the ensemble-averaged (over 27 initial conditions) heat-current autocorrelation as a function of time, and its integral for the $10 \times 10 \times 10$ supercell. Vertical units for the integrated autocorrelation are in W/mK, and the autocorrelation (blue dots) has been multiplied by a constant to be on scale.

we have plotted such an ensemble average for a $10 \times 10 \times 10$ supercell containing 8000 atoms. The error bars are mainly due to the ensemble averaging, and those related to the time averaging are small, as the number of MD time steps are quite large.

We can also see in this figure the cumulative integral of the ensemble-averaged autocorrelation function. The same calculation was performed in a $7 \times 7 \times 7$ supercell of 2744 atoms, where the averaging was over 99 runs with different initial conditions. Due to its larger size, there are smaller fluctuations in the average current per atom in the $10 \times 10 \times 10$ supercell, and we only used 27 initial conditions for this supercell. Since from each MD run one can really extract three autocorrelation functions, κ_{xx}, κ_{yy}, and κ_{zz}, which are equal by cubic symmetry, we also averaged over the three directions. In this sense, the above-mentioned numbers should be multiplied by three.

The error bars are determined by the large fluctuations in the integrated autocorrelations divided by the square root of the number of ensembles. The error bar due to the time average is usually much smaller if MD simulations are run for a long enough time.

The results for two different supercell sizes are summarized in Table II compared with the experimental data of Slack *et al.*[29] One can notice an underestimation of the experimental data, which is reduced as the supercell size is increased. To get the correct value in the thermodynamic limit, one needs to extrapolate these results to infinite size.

There are a few competing effects which can explain this discrepancy: the most important one is size effect, which as was just explained, underestimates κ. Similarly, the larger value of the Gruneisen parameter for the acoustic modes in our model will produce a smaller relaxation time [see the Klemens formula in Eq. (8)].

TABLE II. Thermal conductivity at $T = 600$ K from GK-MD compared to lattice dynamics in the classical limit $[n(\omega) \to k_B T/\hbar\omega]$ with an equivalent number of k-point mesh, and experiment for two different supercell sizes.

Supercell size	MD-GK	LD	Experiment
$7 \times 7 \times 7$	37 ± 10	32.67	64 ± 3
$10 \times 10 \times 10$	43 ± 12	47.2	64 ± 3

The following effects will, however, lead to an overestimation of the thermal conductivity: in the classical MD simulations, the number of modes is the high-temperature limit of the Bose-Einstein distribution, $k_B T/\hbar\omega_{k\lambda}$, which is larger than the quantum distribution. This leads to a heat capacity per mode of k_B and, therefore, an overestimate of the true heat capacity [see also Fig. (8)]. In a finite-size cell, the allowed frequencies are quantized and energy conservation after a three-phonon process can never be exactly satisfied; this will lead to an effectively longer lifetime for phonons, and thus also overestimate κ. It is not easy to quantify these errors, except for those due to the phonon occupation numbers. It is therefore possible that there is a cancellation. In our case, since only two supercell sizes were considered, we cannot do a systematic size scaling study, but overall, due to these cancellations, the GK-MD results seem to be weakly dependent on size, which is in agreement with previous MD simulations (see, for example, Table I in Ref. 11).

Here, we must point out some discrepancies between published results on Si using the SW potential. Using the GK-MD method, Philpot *et al.* and Volz *et al.*[8,9] find a thermal conductivity in reasonable agreement (to within 30%) with experiments. Broido *et al.*,[12] on the other hand, have shown by solving the Boltzmann equation beyond the RTA that $\kappa_{\mathrm{SW}} \geqslant \approx 4\kappa_{\mathrm{experiment}}$. Recently, Sellan *et al.*[11] investigated size effects in GK-MD simulations using the direct method, and also used lattice dynamics to compute the thermal conductivity of Si from the SW potential. They found that $\kappa_{\mathrm{LD}}(T = 500\ \mathrm{K}) = 132/\mathrm{W/mK}$, which is only 70% larger than the experimental value of 80 W/mK, in contrast to the Broido *et al.*[12] prediction. Their direct method, followed by scaling, predicts 93 ± 18 W/mK, and their unscaled GK value for an $8 \times 8 \times 8$ supercell is 231 ± 57 W/mK.

All these results point to the subtleties involved in extracting a reliable value for the thermal conductivity of bulk materials, no matter what method is used.

To investigate this discrepancy, we used our approach to extract harmonic and cubic force constants from the SW potential and used LD theory to compute the corresponding thermal conductivity. Using the same k-point mesh in order to avoid systematic errors, in comparison to FP-derived force constants, we found that at 150 K, the thermal conductivity derived from SW is 80% larger than the one derived from FP-DFT calculations.

C. Phonons, DOS, and Gruneisen parameters

In extracting the force constants, we have limited the range of the harmonic FCs to five neighbor shells, and that of the cubic and quartic terms to one neighbor shell, so that MD

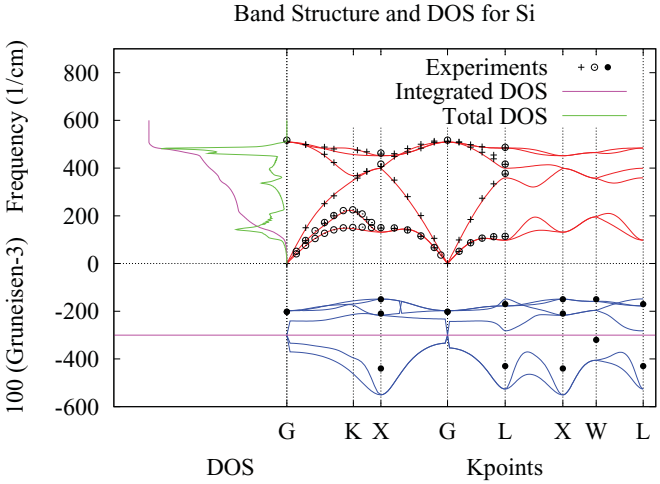

FIG. 3. (Color online) Phonon band structure of Si using force constants up to the fifth neighbor shell. Plus signs represent experimental data of Nelin and Nilsson.[30] Left portion of figure shows the DOS, and right portion of figure shows the rescaled Gruneisen parameters $[100 \times (\gamma - 3)]$.

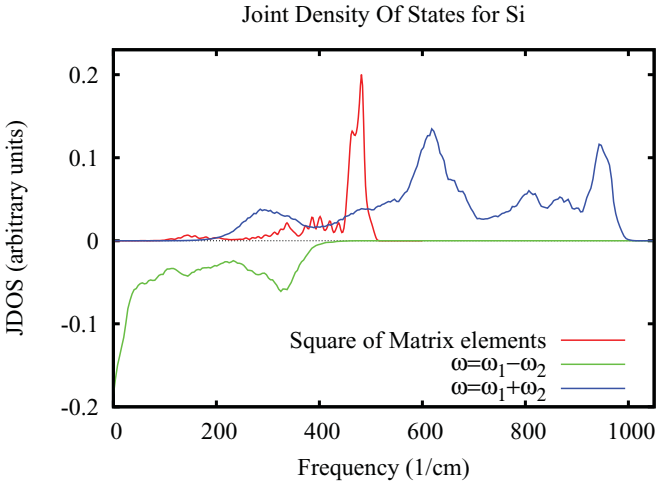

FIG. 4. (Color online) Top line in blue is the DOS associated with two-phonon creation or annihilation (DOS_2^-), and bottom line in green is the DOS associated with one-phonon emission or absorption (DOS_2^+). The red line is the contribution of the matrix elements defined in Eq. (19). The peak at 500 cm^{-1} is the main reason for smaller lifetimes of optical modes.

simulations can be done within a reasonable time. Using the harmonic FCs, we can obtain the phonon spectrum. As can be seen in Fig. 3, the speeds of sound and most of the features are reproduced with very good accuracy. It is well known that in order to reproduce the flat feature in the transverse acoustic (TA) modes near the X point, one must go well beyond the fifth neighbor. For the band structure and the density of states (DOS), the overall agreement is good, except for the Gruneisen parameters of the TA branch, where our calculations, which only include cubic force constants up to the first neighbor shell, overestimate $\gamma(X,\mathrm{TA})$. Based on Klemens' formula [Eq. (8)], one might anticipate that our model will slightly underestimate the lifetime of TA modes and thus their contribution in the thermal conductivity.

D. Phonon lifetimes and mean-free paths

To get an idea of the relative contributions of the matrix elements representing the strength of the three-phonon interactions versus the phase space available for these transitions characterized by the two-phonon DOS, we show in Fig. 4 the plots of these quantities. We define the contribution of the matrix elements as

$$F(\omega) = \sum_{k\lambda} \delta(\omega - \omega_{k\lambda}) \sum_{1,2} |V(k\lambda,1,2)|^2. \qquad (19)$$

From Fig. 4, we can note that optical phonons have a much larger weight coming from the matrix element $|V(k\lambda,1,2)|^2$. This explains why they have such a larger relaxation rate compared to acoustic modes for which the contribution of matrix elements is very small. The two-phonon DOS is representative of the phase space available for the transitions, and is defined as

$$\mathrm{DOS}_2^{\pm}(\omega) = \sum_{1,2} \delta(\omega - \omega_1 \pm \omega_2). \qquad (20)$$

From Fig. 4, it can be inferred that one-phonon absorption or emission (DOS_2^+) dominates for low-frequency phonons (acoustic), while two-phonon absorption or emission (DOS_2^-) dominates at high frequencies (LA and optical).

Next, we show in Fig. 5 the calculated lifetimes of the three acoustic and optical modes versus frequency for a regular mesh of k-points in the first Brillouin zone, at $T = 70$ and

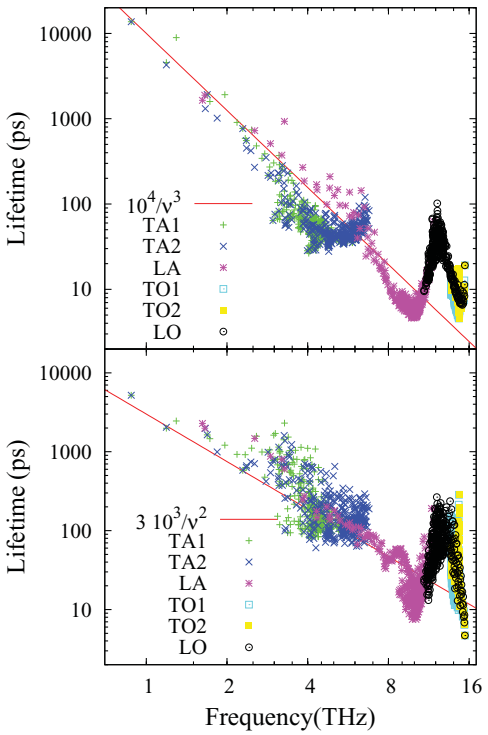

FIG. 5. (Color online) Lifetimes of the six branches in Si at 277 K vs. frequency on a logarithmic scale. Top plot is for umklapp and bottom plot is for normal processes. The quadratic dependence of the acoustic modes can be noticed for normal processes, while umklapp processes seems to scale as $1/\omega^3$.

277 K. The results depend slightly on the number of k-point mesh used for the integration within the FBZ. Here, we are showing results obtained with $18 \times 18 \times 18$ mesh, which is close to convergence. The normal and umklapp components of the lifetimes are separated as $1/\tau = 1/\tau^U + 1/\tau^N$. We note that although the lifetimes associated with normal processes are in $1/\omega^2$, those of umklapp processes seem to scale at low frequencies like $1/\omega^3$, so that the former dominates at low frequencies. This is in contrast to the first-principles results provided by Ward and Broido,[31] who report that the umklapp rate is in ω^4. Although not explicitly mentioned in their paper,[32] fits to their data with ω^3 were almost as good as the fit with ω^4. In the Appendix, we provide a proof of why, in the case of Si, the umklapp rate would behave as ω^3.

From Fig. 5, we can notice that at low frequencies (typically below 3 THz or 100 cm^{-1} where dispersions are linear), normal rates dominate, while at higher frequencies and typically for optical modes, umklapp processes dominate transport.

E. Thermal conductivity from lattice dynamics

To see the contribution of each MFP to the total thermal conductivity, following the approach of Dames and Chen,[33] we have decomposed the thermal conductivity based on each mode and sorted each component according to their mean-free paths. One can then define a differential thermal conductivity and the accumulated one, which is its integral:

$$d\kappa(\Lambda_{k\lambda}) = \frac{1}{3} v_{k\lambda}\, \Lambda_{k\lambda}\, C_{v k\lambda},$$
$$\kappa(\Lambda) = \frac{1}{N_k} \sum_{k\lambda}^{\Lambda_{k\lambda}<\Lambda} d\kappa(\Lambda_{k\lambda}). \tag{21}$$

The above can be plotted versus the MFP, Λ, which can be considered as an independent variable. Figure 6 shows such contribution at 277 K. By considering the extrapolated value to

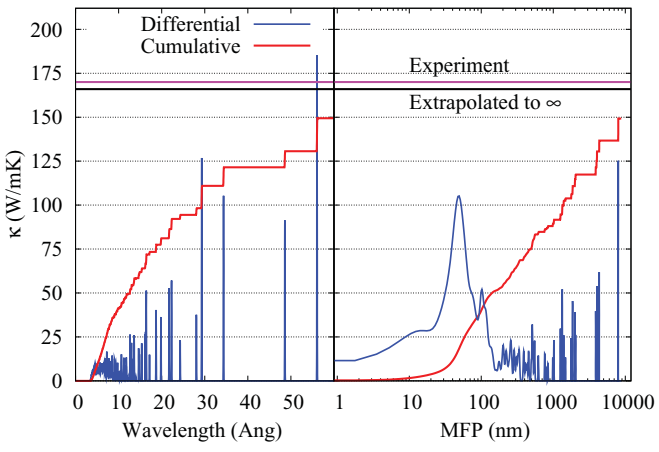

FIG. 6. (Color online) Cumulative contributions of phonons to the thermal conductivity at 277 K from the $18 \times 18 \times 18$ k-point mesh data. Left plot is according to the wavelengths, and right plot is according to the MFPs. Both differential and cumulative thermal conductivities are shown in blue and red, respectively. For comparison, the extrapolated (to infinite k-point mesh) and experimental κ are also shown with horizontal lines at 166 and 174 W/mK, respectively.

be 166 W/mK, one can notice that MFPs extend well beyond 10 microns, even at room temperature. Surprisingly, MFPs longer than 1 micron contribute to almost half of the total thermal conductivity. One should also note that the range of MFPs, in Si at least, span over five orders of magnitude from a nanometer to 100 microns at room temperature. This would be larger as we go to lower temperatures.

To get an accurate estimate of the thermal conductivity, one needs to extrapolate the data obtained from a finite number of k-point mesh, according to Eq. (9). The extrapolated thermal conductivity versus temperature is plotted in Fig. 7 and compared to the experimental results of Glassbrenner and Slack[29] and Inyushkin *et al.*[34] We can notice that at low temperatures, boundary scattering limits the experimental thermal conductivity. The agreement is very good in the temperature range of 100 to 500 K, after which experimental results decay faster due to higher-order phonon scatterings, which are $1/T^2$ or higher. Our results are within the relaxation-time approximation, but one could also go beyond and iteratively solve the Boltzmann equation, as Broido *et al.* have done.[16] They have shown that for Si and Ge, there would be about a further 10% increase in κ.

To assess the effect of the classical approximation, which is made in classical MD simulations, we have also compared in Fig. 8, for a given k-point density, the classical and the quantum thermal conductivities within the RTA. They are displayed with symbols on the lines. The quantum one is given by Eq. (16), and the classical one uses the same expression in which the Bose-Einstein distribution is substituted by $k_B T/\hbar\omega$, both in the heat capacity and in the relaxation time. We can notice that the difference is small above the Debye temperature, as expected, but the classical value overestimates the quantum one by 10% to 20% as the temperature is lowered further. This is a combination of the larger heat capacity and a smaller lifetime in the classical case. We have also plotted the contribution of each mode to the thermal conductivity. We can note that at low temperatures mainly, the two TA modes equally contribute to κ, whereas at temperatures above 200 K, LA and TA modes equally contribute about almost 1/3 of the

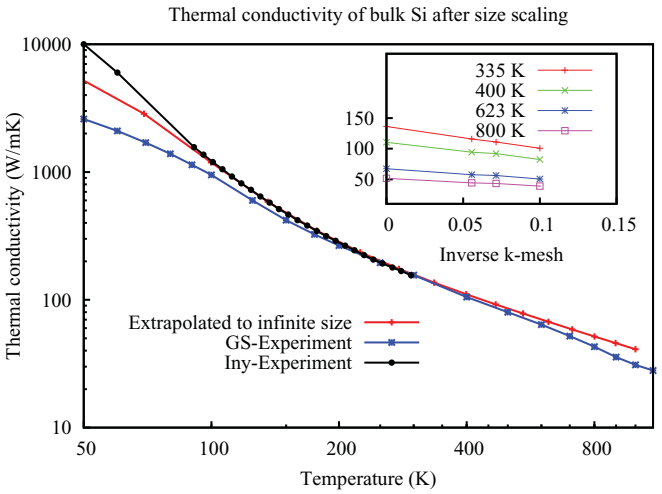

FIG. 7. (Color online) Thermal conductivity of pure Si crystal from Eq. (16) vs. temperature. Inset: Extrapolation to infinitely dense k-points.

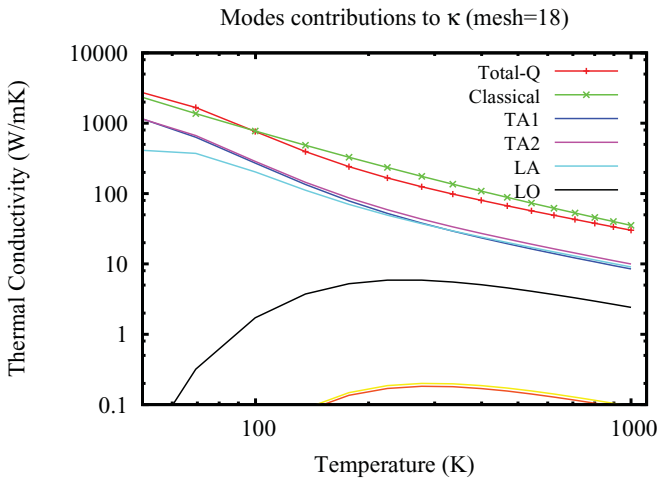

FIG. 8. (Color online) Quantum and classical thermal conductivities of Si vs. temperature [from Eq. (16) with k-point mesh = 18]. The contribution of each mode is also being plotted.

thermal conductivity, while the longitudinal optic contribution is about 5%.

The computation of the thermal conductivity using the RTA is to some extent more straightforward than the use of GK-MD. The former involves a double summation in the FBZ and has very little systematic error in it, whereas the MD simulations require an ensemble-averaging process with a relatively large error bar, not to mention the much longer CPU time needed to run the MD simulations.

For a mesh of k-points equal to the number of primitive cells included in the MD supercell, we have obtained agreement between MD results and the classical version of Eq. (16), as also shown in Table II.

VI. CONCLUSIONS

Using first-principles calculations, we developed a classical force field, which was used both in a molecular dynamics simulation and in the calculation of anharmonic phonon lifetimes. Both methods provided an estimate for the thermal conductivity of pure crystalline silicon. The results of these two methods agreed for the same system size in the case where $\kappa_{\rm LD}$ was evaluated in the classical limit. GK-MD is, however, much more time consuming and includes large statistical errors. Furthermore, it does not provide much information besides the way the integrated autocorrelation converges with simulation time. Size effects were discussed and arguments were provided as to why equilibrium MD simulations converged relatively fast with respect to the supercell size. Lattice dynamics, on the other hand, proved to be faster, more accurate, and contain more useful information. The use of a linear extrapolation versus the inverse of the size led to a surprisingly good agreement with experiments. Such extrapolation is justified for relaxation rates that are quadratic in frequency at low frequencies. The decomposition of κ into the contribution of different mean-free paths showed that, in Si, MFPs span over five orders of magnitude from 1 nm to 100 microns at room temperature, where about half of the thermal conductivity comes from MFPs larger than 1 micron.

The developed potential has the advantage of being amenable to systematic improvement by including more neighbor shells at the cost of heavier calculations. The approach of using the FGR for the estimation of relaxation rates and the RTA, or an improved approximation to κ by solving the linearized Boltzmann equation, allows one to obtain a relatively accurate estimate of the thermal conductivity of an arbitrary bulk crystalline structure from a few force-displacement relations obtained using first-principles calculations, without any fitting parameters. This method paves the way for an accurate prediction of thermal properties of nanostructured or composite materials in a multiscale approach, which takes as input the relaxation times due to anharmonicity and defect scatterings.

ACKNOWLEDGMENTS

The authors wish to acknowledge useful discussions with Junichiro Shiomi, Joseph Feldman, Peter Young, and Asegun Henry. We thank Nuo Yang for providing the SW force-displacement data used in Fig. 1.

This work was supported as part of the Solid-State Solar-Thermal Energy Conversion Center (S^3TEC), an Energy Frontier Research Center funded by the US Department of Energy, Office of Science, Office of Basic Energy Sciences (Grant No. DE-SC0001299).

APPENDIX

In this Appendix, we show the frequency dependence of the umklapp rates. According to Eq. (12), the relaxation rate is a product of the three-phonon matrix element $|V(q\lambda,1,2)|^2$, a combination of occupation factors, and δ functions reflecting the constraints of energy conservation. We will separately discuss the frequency dependence of the matrix element and the phase space term.

First, the sum over the second momentum 2 is canceled by the constraint of momentum conservation, so that the relaxation rate is just the 3D integral over q_1 in the FBZ. One of the dimensions can be integrated over by using the identity

$$\begin{aligned}\int d^3q_1\,\delta\left(\omega+\omega_{q_1\lambda_1}-\omega_{q_2\lambda_2}\right)f(q_1\lambda_1)\\ =\int d^3q_1\,\delta(q_1-q_o)/\left|v_{q_1\lambda_1}-v_{q+q_1\lambda_2}\right|f(q_1\lambda_1)\\ =\int d^2S_{q_o}1/\left|v_{q_o\lambda_1}-v_{q+q_o\lambda_2}\right|f(q_o\lambda_1),\end{aligned}\tag{A1}$$

where q_o is the solution of $\omega_{q\lambda}+\omega_{q_o\lambda_1}-\omega_{-q-q_o\lambda_2}=0$. Note that the denominator containing the group velocities is not small, as long as λ_1 and λ_2 refer to 2 different branches; but in the case $\lambda_1=\lambda_2$, the denominator becomes linear in q.

Second, for umklapp processes, in the small ω limit, we must have both q_1 and $q_2=-q-q_1$ near the Brillouin zone boundary, such that q_1 is inside the zone and q_2 is outside, so that the corresponding frequencies are not infinitesimally small, but their difference would be. In general, this forces the q_1 surface integral to be limited to a pocket of dimensions q located at the FBZ boundary, so that the surface integral is of

the order of q^2. But in the case where there is a degenerate band at the zone boundary, the surface would be of the order of q instead. Different cases based on the symmetry of the crystal and the type of degeneracy have been discussed in detail by Herring.[35] In our case of interest, namely Si, it is possible to have a three-phonon process involving a small-momentum q acoustic mode connecting the LA branch to the LO one, with which it is degenerate, near the Brillouin zone boundary all along $X \rightarrow W$, with a surface area S_{q_o}, of the order of q.

Third, among the two types of terms, i.e., phonon ω decaying to $\omega_1 + \omega_2$ and one phonon absorption $\omega + \omega_1 = \omega_2$, the former cannot contribute because $\omega \simeq 0$ and ω_1 and ω_2 are finite. Therefore, only the terms $(n_2 - n_1) \times [\delta(\omega_1 - \omega_2 + \omega) - \delta(\omega_1 - \omega_2 - \omega)]$ contribute to the umklapp lifetimes at small frequencies. In the latter, one can substitute $n_1 - n_2$ by $\pm\omega\, \partial n/\partial\omega_1 \simeq O(q)$. We must remember to substitute the argument ω in the relaxation rate by its on-shell value $\omega_q = v \times q \rightarrow 0$, so that in the limit of low frequencies, the inverse lifetime can be written as

$$\int d^2 S(q_o)\, \frac{1}{\left| v_{q_o\lambda_1} - v_{q+q_o\lambda_2} \right|}\, \omega_{q\lambda}\, \frac{\partial n}{\partial \omega_o} |V(q, q_o, -q - q_o)|^2. \tag{A2}$$

Finally, due to the odd parity of the cubic force constants, one can show that for small q, we have $|V(q,q_o,-q-q_o)| \propto \sin q R/\sqrt{\omega_q} \propto \sqrt{q}$.

Putting everything together, we find that the umklapp rates at low frequencies are, to leading order, of the form

$$\frac{1}{\tau^U(\omega)} \propto q^3 \propto \omega^3. \tag{A3}$$

This is in agreement with our numerical findings.

For normal processes, there is no restriction for modes 1 and 2 to be near the BZ boundary. For instance, in the (LA $\rightarrow$ LA + TA) process, the term $(1 + n_1 + n_2)$ contributes and will not be linear in q. In such cases, the rate would be in q^2 and would dominate umklapp terms with higher powers of q.

[1] F. H. Stillinger and T. A. Weber, Phys. Rev. B **31**, 5262 (1985).

[2] G. C. Abell, Phys. Rev. B **31**, 6184 (1985); J. Tersoff, *ibid.* **38**, 9902 (1988); D. W. Brenner, *ibid.* **42**, 9458 (1990).

[3] M. C. Payne, M. P. Teter, D. C. Allan, T. A. Arias, and J. D. Joannopoulos, Rev. Mod. Phys. **64**, 1045 (1992).

[4] R. Car and M. Parrinello, Phys. Rev. Lett. **55**, 2471 (1985).

[5] M. S. Green, J. Chem. Phys. **22**, 398 (1954).

[6] R. Kubo, J. Phys. Soc. Jpn. **12**, 570 (1957).

[7] One reason for the success of the SW potential compared to others is its ability to reproduce a relatively correct Gruneisen parameter and thermal expansion coefficient. It is not clear to us whether or not this is accidental, as the way SW determined their parameters was not clarified in their paper. The properties of the SW and Tersoff potential have been discussed by Porter *et al.*, J. Appl. Phys. **82**, 5381 (1997).

[8] S. G. Volz and G. Chen, Phys. Rev. B **61**, 2651 (2000).

[9] P. K. Schelling, S. R. Phillpot, and P. Keblinski, Phys. Rev. B **65**, 144306 (2002).

[10] A. Henry and G. Chen, J. Comput. Theor. Nanosci. **5**, 141 (2008).

[11] D. P. Sellan, E. S. Landry, J. E. Turney, A. J. H. McGaughey, and C. H. Amon, Phys. Rev. B **81**, 214305 (2010).

[12] D. A. Broido, A. Ward, and N. Mingo, Phys. Rev. B **72**, 014308 (2005).

[13] Sun and J. Murthy, Appl. Phys. Lett. **89**, 171919 (2006).

[14] J. A. Pascual-Gutierrez, J. Murthy, and R. Viskanta, J. Appl. Phys. **106**, 063532 (2010).

[15] Private communication with the referee.

[16] D. A. Broido, M. Malorny, G. Birner, N. Mingo, and D. A. Stewart, Appl. Phys. Lett. **91**, 231922 (2007).

[17] K. Esfarjani and H. T. Stokes, Phys. Rev. B **77**, 144112 (2008).

[18] M. Sluiter, M. Weinert, and Y. Kawazoe, Europhys. Lett. **43**, 183 (1998); M. H. F. Sluiter, M. Weinert, and Y. Kawazoe, Phys. Rev. B **59**, 4100 (1999).

[19] QUANTUM ESPRESSO is an electronic structure package based on the density functional theory developed at SISSA. The methodology is detailed in P. Giannozzi *et al.*, J. Phys. Condens. Matter **21**, 395502 (2009).

[20] N. Mingo, K. Esfarjani, D. A. Broido, and D. A. Stewart, Phys. Rev. B **81**, 045408 (2010).

[21] R. Prado, *Time Series: Modeling, Computation, and Inference*, CRC Texts in Statistical Science (Chapman and Hall, London, 2010), Vol. 86.

[22] P. G. Klemens, in *Thermal Conductivity*, edited by R. P. Tve (Academic, London, 1969), Vol. 1.

[23] J. E. Turney, E. S. Landry, A. J. H. McGaughey, and C. H. Amon, Phys. Rev. B **79**, 064301 (2009).

[24] A. A. Maradudin and A. E. Fein, Phys. Rev. **128**, 2589 (1962).

[25] R. A. Cowley, Rep. Prog. Phys. **31**, 123 (1968).

[26] G. P. Srivastava, *The Physics of Phonons* (Taylor and Francis, London, 1990).

[27] J. A. Reissland, *The Physics of Phonons* (Wiley, New York, 1973).

[28] J. P. Perdew and A. Zunger, Phys. Rev. B **23**, 5048 (1981).

[29] C. J. Glassbrenner and G. A. Slack, Phys. Rev. **134**, A1058 (1964).

[30] G. Nelin and G. Nilsson, Phys. Rev. B **5**, 3151 (1972).

[31] A. Ward and D. A. Broido, Phys. Rev. B **81**, 085205 (2010).

[32] After private communication with D. Broido, we found out that their low-frequency data could as well be fitted with ω^3, and their choice of ω^4 was because of a better agreement in some intermediate frequency range.

[33] C. Dames and G. Chen, *Thermal Conductivity of Nanostructured Thermoelectric Materials, CRC Handbook*, edited by M. Rowe (Taylor and Francis, Boca Raton, FL, 2006).

[34] A. V. Inyushkin, A. N. Taldenkov, A. M. Gibin, A. V. Gusev, and H.-J. Pohl, Phys. Status Solidi C **11**, 2995 (2004).

[35] C. Herring, Phys. Rev. **95**, 954 (1954).